

C6.2 class flare parameters inferred with a 3D geometry of flare database

Valente A. Cuambe^{1,2,#}, J. E. R. Costa³, P. J. A. Simões⁴

valente.a.cuambe@a-raege-az.pt

¹AIR CENTRE - Atlantic International Research Centre

²RAEGE - Rede Atlantica de Estacoes Geodinamicas e Espaciais

³INPE - Astrophysics Division, National Institute for Space Research

⁴CRAAM- Mackenzie, Escola de Engenharia, Universidade Presbiteriana Mackenzie

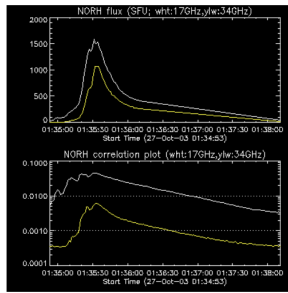
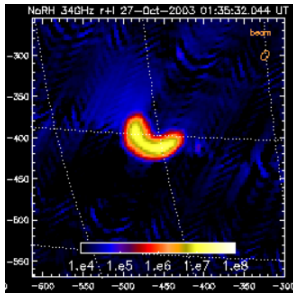
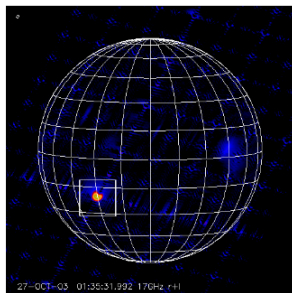
#CICGE, DGAOT, FCUP, Vila Nova de Gaia, Portugal

August 3, 2023

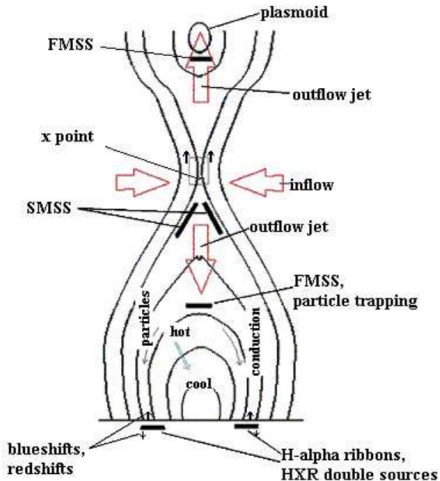


Motivation

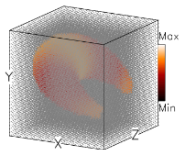
- GOES C6.2 class flare occurred on 27 October 2003 at heliographic position S20E29 in the active region NOAA 486. This flare shows a typical loop-like geometry and presents a simple structure.
- We aim to explore the unknown parameters by implementing the forward-fitting method using an optimised database of a 3D magnetic loop geometry.



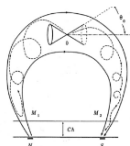
- The standard model [Kopp and Pneuman, 1976]
- Solar flares often exhibit two bright, elongated regions known as flare ribbons
- The reconnection of magnetic field lines occurs at the top of the loop
- Particles precipitates along magnetic loop and hit the chromosphere footpoints



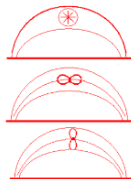
[Simões and Costa, 2006, Simões and Costa, 2010, Costa et al., 2013, Cuambe et al., 2018]



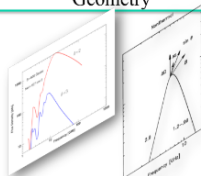
Geometry



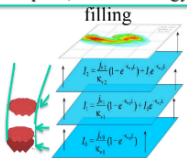
Space, time & energy



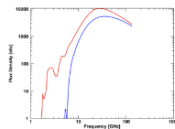
Non stationary evolution



Emission Mechanisms



Radiation Transfer

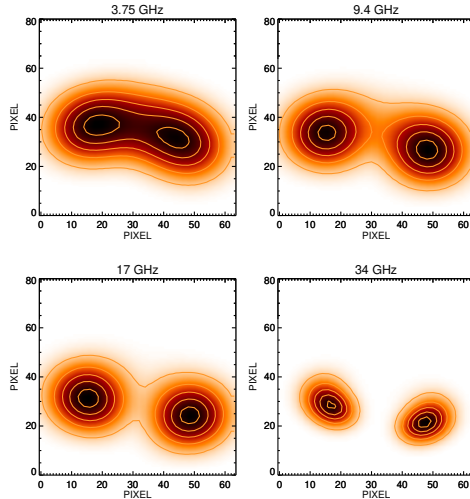
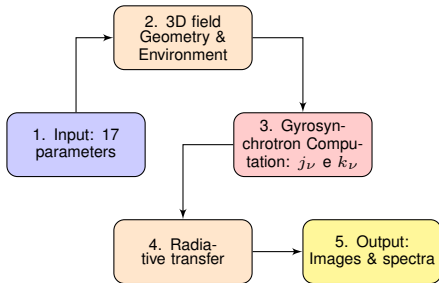


Medium Influence

- Box with 16x16x16 voxels
- Z – viewer direction
- X – Solar equator
- Y – rotation axis

- Any heliographic position
- Top cross section variable
- Foot separation variable
- Loop height and inclination variable

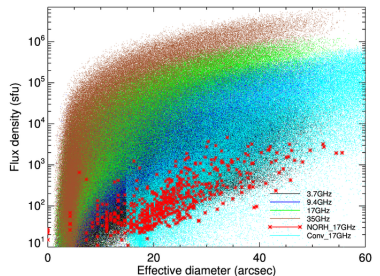
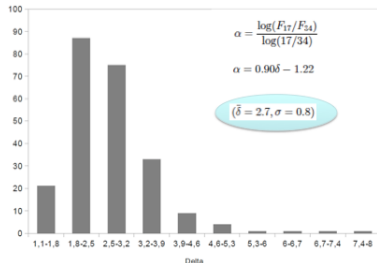
- Magnetic field (dipole)
- Viewing angle
- Ambient temperature
- Ambient density
- Electron density (Nel)



- **Energy:**
- $\Rightarrow 10 \text{ keV} - 100 \text{ MeV}$
- **ambient density:**
- $\Rightarrow 10^9 - 10^{14} \text{ cm}^{-3}$
- **Nonthermal eletron number density**
[Lee et al., 2009]:
- $\Rightarrow 7 \times 10^{34} - 3 \times 10^{42}$.

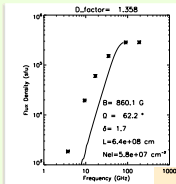
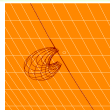
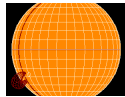
Tabela 6.1 - Intervalo de parâmetros no banco de modelos

| No. | Parâmetro | min | max | Símbolo | Unidade |
|-----|------------------------|-----------------|-----------------|------------------|------------------|
| 1 | Preenchimento do arco | 0.2 | 2 | ω | - |
| 2 | Delta | 1. | 4.4 | δ | - |
| 3 | Densidade dos elétrons | 1×10^6 | 1×10^8 | Nel | cm^{-3} |
| 4 | Assimetria | -50 | 50 | As | % |
| 5 | Azimute | -90 | 90 | Az | Grau |
| 6 | Raio do ápice | 0.002 | 0.02 | R_{arc} | R_{\odot} |
| 7 | Separação dos pés | 0.008 | 0.06 | $Foot_s$ | R_{\odot} |
| 8 | Altura | 0.008 | 0.06 | H_{arc} | R_{\odot} |
| 9 | Inclinação | -40 | 40 | Inc | Grau |
| 10 | Campo magnético | 800 | 3500 | B | Gauss |



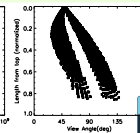
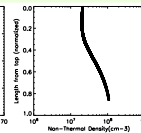
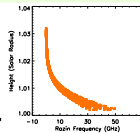
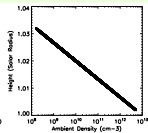
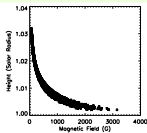
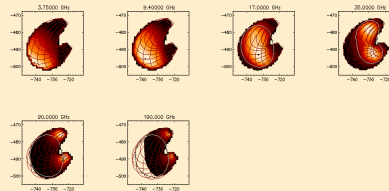
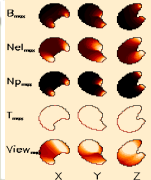
nnhome/valente/Dropbox/Programas_Valente/ModelosV/img_p-60az-60lat-30c007par0np2fr003700930170035009001900

REPORT



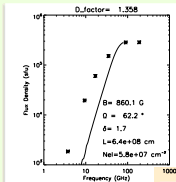
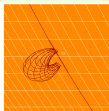
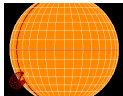
| DATA | MIN | MAX | MEAN |
|----------|----------|----------|----------|
| B | 63. | 3152. | 305. |
| Nel | 2.03E+07 | 1.08E+08 | 3.00E+07 |
| Np | 1.66E+08 | 4.99E+12 | 1.61E+11 |
| T | 1.00E+08 | 1.00E+08 | 1.00E+08 |
| View | 28. | 137. | 63. |
| Energy | 10. | 100000. | 347.0 |
| δ | 1.7 | 1.7 | |

| | |
|-------------|-------|
| Latitude | -30.0 |
| Longitude | -60.0 |
| Azimuth | -60.0 |
| Height | 0.020 |
| Radius | 0.010 |
| Foot Sep. | 0.020 |
| Elect. Fill | Homog |



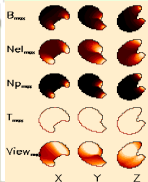
nnhome/valente/Dropbox/Programas_Valente/ModelosV/img_p-60az-60lat-30c007par0np2fr003700930170035009001900

REPORT



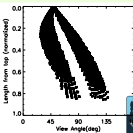
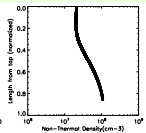
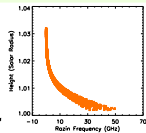
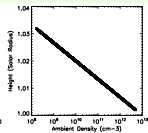
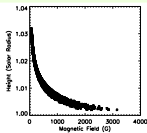
| DATA | MIN | MAX | MEAN |
|--------|----------|----------|----------|
| B | 63. | 3152. | 305. |
| Nel | 2.03E+07 | 1.08E+08 | 3.00E+07 |
| Np | 1.66E+08 | 4.99E+12 | 1.61E+11 |
| T | 1.00E+08 | 1.00E+08 | 1.00E+08 |
| View | 28. | 137. | 63. |
| Energy | 10. | 100000. | 347.0 |
| δ | 1.7 | 1.7 | |
| | | | |
| | | | |

| | |
|-------------|-------|
| Latitude | -30.0 |
| Longitude | -60.0 |
| Azimuth | -60.0 |
| Height | 0.020 |
| Radius | 0.010 |
| Foot Sep. | 0.020 |
| Elect. Fill | Homog |
| | |
| | |

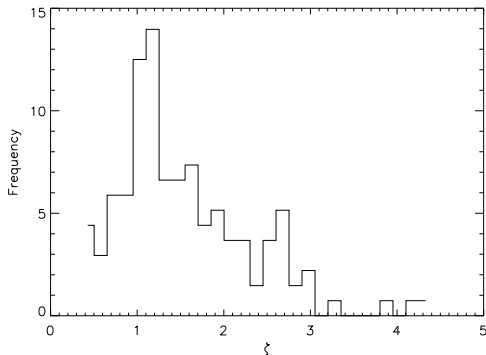


$$\chi^2 = \sum \frac{1}{\sigma_{\psi_{Obs_i}}^2} (\psi_{Mod_i} - \psi_{Obs_i})^2 \quad (1)$$

$$\zeta = \sum_{i=1}^{10} \left(\frac{|Par_i^{Sim} - Par_i^{Res}|}{|Par_i^{max} - Par_i^{min}|} \right) \quad (2)$$



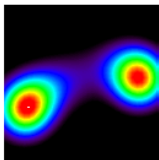
- The parameters recovering in the database were tested in randomly simulated flares.
- 56% of the simulations shows satisfactory results.
- More than 50% of the parameters were recovered with $\zeta \leq 10\%$.



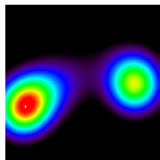
We evaluate the following:

- Simulations with $|\zeta| < 1.2$
- Simulations with $|\zeta| \sim 1.2$
- Simulations with $|\zeta| > 1.2$

SIMULATION



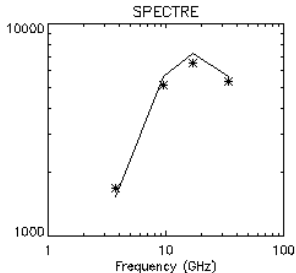
SOLUTION



COMPARED PARAMETERS

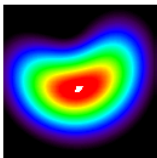
$i_e = 0.30$
 $\Delta = 3.98$
 $Assim = -0.05$
 $N_e = 9.333e+06$
 $Azím = 0.00$
 $Raio = 0.01$
 $Foot = 0.03$
 $h_arc = 0.02$
 $Incl = -40.00$
 $Bmag = 1716.43$

$i_e = 0.30$
 $\Delta = 3.59$
 $Assim = 0.00$
 $N_e = 1.778e+06$
 $Azím = -15.00$
 $Raio = 0.01$
 $Foot = 0.03$
 $h_arc = 0.02$
 $Incl = -40.00$
 $Bmag = 1389.58$

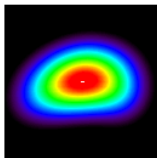


$i_e = 0.00$
 $\Delta = 0.11$
 $Assim = 0.05$
 $N_e = 7.631e-02$
 $Azím = 0.17$
 $Raio = 0.11$
 $Foot = 0.00$
 $h_arc = 0.00$
 $Incl = 0.00$
 $Bmag = 0.12$
 $yy = 0.640$

SIMULATION



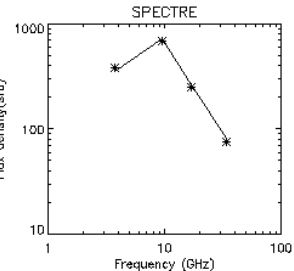
SOLUTION



COMPARED PARAMETERS

ie= 1.20
 Delta= 2.47
 Assim= -0.05
 Ne= 1.349e+07
 Azim= 0.00
 Raio= 0.01
 Foot= 0.05
 h_arc= 0.04
 Incl= 0.00
 Bmag=1492.45

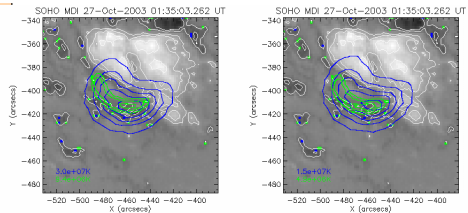
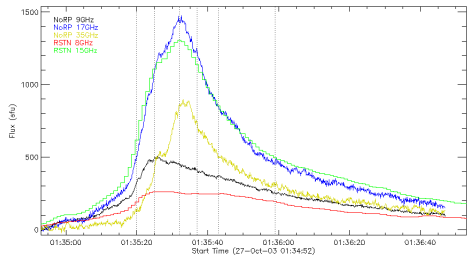
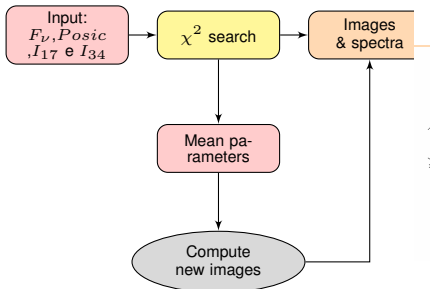
ie= 0.30
 Delta= 2.74
 Assim= -0.50
 Ne= 1.778e+07
 Azim= 0.00
 Raio= 0.01
 Foot= 0.05
 h_arc= 0.04
 Incl= 0.00
 Bmag=1244.98



ie= 0.50
 Delta= 0.08
 Assim= 0.45
 Ne= 4.337e-02
 Azim= 0.00
 Raio= 0.11
 Foot= 0.00
 h_arc= 0.00
 Incl= 0.00
 Bmag= 0.09
 yy= 1.275

Table: Fitting parameters for flux calculations.

| Time (UT) | Peak (GHz) | α_{thick} | α_{thin} |
|-----------|------------|------------------|-----------------|
| 01:35:20 | 12.44 | 1.35 | -2.32 |
| 01:35:25 | 12.84 | 1.52 | -1.14 |
| 01:35:32 | 17.76 | 1.95 | -0.82 |
| 01:35:37 | 17.01 | 1.98 | -0.81 |
| 01:35:43 | 11.43 | 1.57 | -0.67 |
| 01:35:59 | 10.19 | 1.09 | -0.49 |



$$S = A\nu^a(1 - e^{-B\nu^{-b}}) \quad (3)$$

[Stahli et al., 1989]

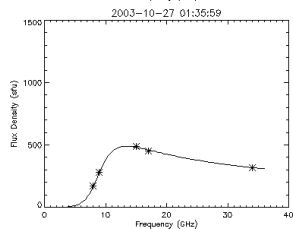
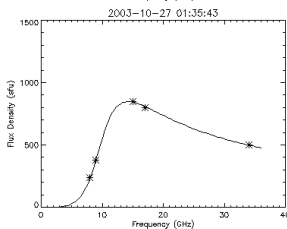
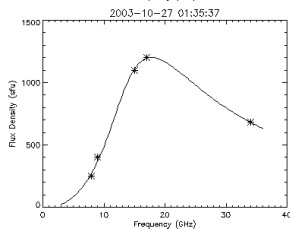
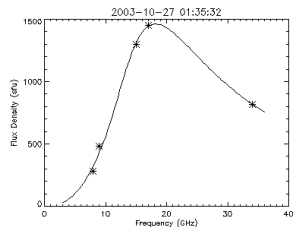
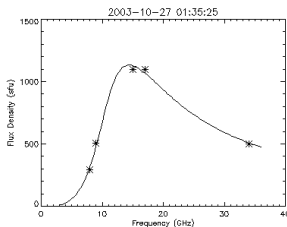
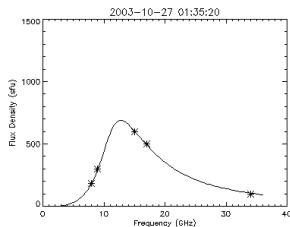
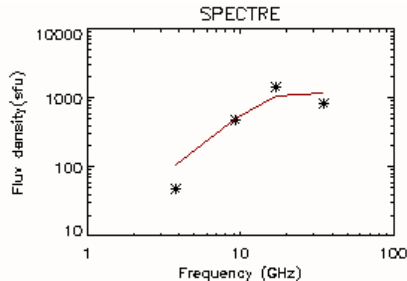
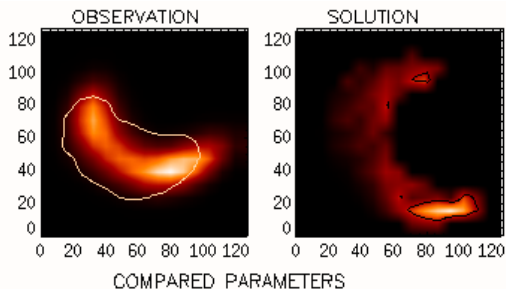
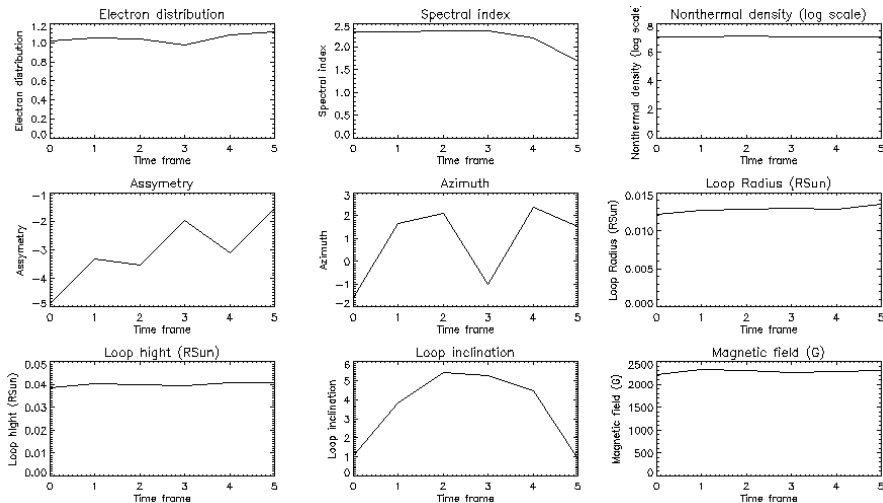


Table: Parameters of the database solutions.

| Time (UT) | Parameters | | | | | | | | | |
|-----------|------------|-----------------|-------------------------------|----------|-----------|-------------------------|-------------------------|-------------------------|----------|-----------|
| | ie (1) | δ (2) | $N_{\text{nth}}(\log)$ (3) | q (4) | Az (5) | R_{Arc} (6) | F_{sep} (7) | H_{Arc} (8) | t (9) | B (10) |
| 01:35:20 | 1.02 | 2.32 | 7.08 | -4.90 | -1.58 | 0.01 | 0.03 | 0.04 | 1.07 | 2223.20 |
| 01:35:25 | 1.05 | 2.31 | 7.08 | -3.33 | 1.66 | 0.01 | 0.03 | 0.04 | 3.84 | 2328.55 |
| 01:35:32 | 1.04 | 2.34 | 7.11 | -3.55 | 2.08 | 0.01 | 0.03 | 0.04 | 5.43 | 2308.15 |
| ** | 1.74 | 5.74 | 9.67 | 37.32 | 7.42 | 0.01 | 0.04 | 0.03 | 55.32 | 2543.60 |
| 01:35:37 | 0.97 | 2.34 | 7.10 | -1.95 | -1.00 | 0.01 | 0.03 | 0.03 | 5.27 | 2263.58 |
| 01:35:43 | 1.08 | 2.19 | 7.07 | -3.10 | 2.34 | 0.01 | 0.03 | 0.04 | 4.47 | 2289.33 |
| 01:35:59 | 1.11 | 1.67 | 7.08 | -1.56 | 1.52 | 0.01 | 0.03 | 0.04 | 0.89 | 2299.85 |

** – The refined parameters with the pikaia algorithm.





- Accelerates the search for the best geometric representation of brightness distribution maps from NoRH and the search for the best representation of NoRP spectra.
- The probability of success in the results is directly linked to the growth of the database.
- Additionally, using additional information in different observation bands contributes positively to success.
- The weighted mean solutions are an improvement to address the degeneracy on a single solution with the lowest χ^2 value.
- The weighted mean solutions are employed as an initial guess in different Monte Carlo methods to refine the fitting.

 Costa, J., Simões, P., Pinto, T., and Melnikov, V. (2013).

Solar burst analysis with 3d loop models.
Publication Astronomy Society Japan, 65:5.

 Cuambe, V. A., Costa, J. E. R., and Simões, P. J. A. (2018).

Flare parameters inferred from a 3d loop model database.
Monthly Notices of the Royal Astronomical Society, page 12.

 Kopp, R. and Pneuman, G. (1976).

Magnetic reconnection in the corona and the loop prominence phenomenon.
Solar Phys., 50:85–98.

 Lee, J., Nita, G., and Gary, D. (2009).

Electron energy and magnetic field derived from solar microwave burst spectra.
APJ, 696:274–279.

 Simões, P. and Costa, J. (2006).

Solar bursts gyrosynchrotron emission from three-dimensional sources.
Astronomy & Astrophysics, 453:729–736.

 Simões, P. and Costa, J. (2010).

Gyrosynchrotron emission from anisotropic pitch-angle distribution of electrons in 3-d solar flare sources.
Solar Phys., 266:109–121.

 Stahli, M., Gary, D., and Hurford, G. (1989).

High-resolution microwave spectra of solar bursts.
Solar Phys., 120:351–368.

Thank you !!